Load Adaptability of Active Harmonic Reduction for 12-Pulse Diode Bridge Rectifier With Active Interphase Reactor

Fangang Meng, Wei Yang, *Member, IEEE*, Yi Zhu, Lei Gao, and Shiyan Yang

***Abstract*—In order to improve the harmonic reduction ability of 12-pulse rectifier, an active interphase reactor (AIPR) and corresponding auxiliary circuit are often used to produce circulating current resulting in harmonic reduction. This paper analyzes the load adaptability of 12-pulse rectifier with AIPR. The loads are classified into three types, *RL*-type load, *RC*-type load, and *RLC*-type load. Load currents and circulating currents are calculated under different load types. According to the calculation results, the THD of input line current and ripple coefficient of load voltage are also described by figures under *RL*-type load and *RLC*-type load. The appropriate amplitude of the circulating current under *RL*-type load and the *LC* filter under *RLC*-type load are presented. Simulation and experimental results validate the theoretical analysis.**

***Index Terms*—Active harmonic reduction, active interphase reactor, load adaptability, 12-pulse rectifier.**

I. Introduction

BECAUSE of its simple configuration, low EMI, high reliability, reduced harmonics of input line current, and low ripple of load voltage, multipulse rectifiers (MPR) are widely used in high power rectification [1], [2]. Among MPRs, 12-pulse rectifier is the most popular because its phase-shift transformer has the simplest winding configuration and the highest power density. However, the THD of input line current in 12-pulse rectifier is 15.2% under large inductive load which does not meet the requirement of the harmonics standard [3]. Therefore, how to reduce the harmonics generated by the diode bridges to an acceptable level is a hot topic in MPR research.

In MPRs, pulse number determines the harmonic reduction ability. Therefore, increasing pulse number is one of the design goals in MPR [4]. In general, there are two methods to increase pulse number. One is to augment the output phase number of phase-shift transformer which may increase the winding number and further leads to low power density [5], [6]. Another is to use active or passive harmonic reduction device at the dc or ac mains of MPR to increase pulse number [4], [6]–[16]. For example, in [8] and [11], Choi *et al.* and Lee *et al.* proposed a 12-pulse rectifier using an AIPR at dc side to eliminate harmonics of input line current, respectively. Besides the 12-pulse rectifier with AIPR, there are other 12-pulse rectifiers with the auxiliary circuit of active harmonic reduction at dc side [10], [14], [16]–[23]. In [14], Bai *et al.* proposed a 12-pulse rectifier with current sources formed by two buck-boost converters; in [16], Biela *et al.* proposed a 12-pulse rectifier with a two-switch boost stage to improve sinusoidal input current. The essence of active harmonic reduction at dc side of the 12-pulse rectifier is to use the active devices producing a circulating current to reduce harmonics. Therefore, the circulating current affects the harmonic reduction ability.

The ideal amplitude of the circulating current is half of the instantaneous load current. However, in application, almost all of the analysis about 12-pulse rectifier with active or passive harmonic reduction device is based on large inductive load [3]–[12]. Under large inductive load, load current is assumed to be constant which is very convenient for theoretical analysis. To set the 12-pulse rectifier with AIPR as an example, under large inductive load, the amplitude of the circulating current generated by the auxiliary circuit is half of load current, and the load ripple current is not taken into consideration. Therefore, the amplitude of the circulating current is determined by the load current, and furthermore, is determined by the load types. However, in different application fields, the load types of MPR are different. For example, in engineering application, the more common is that a large capacitor is connected in parallel with the load [6], [13], which can be considered as a *RLC*-type load. Even though for the inductive load, the load smoothing inductance is also rigorously restricted. Therefore, when the circulating current designed under the large inductive load is applied to different load types, the harmonic reduction ability may be affected to some degree. In addition, the load voltage of the MPR using active reduction method usually contains 12 pulses in one cycle, which is not affected by the circulating current. However, if the amplitude of the circulating current is greater than half of the instantaneous load current, the bridge rectifiers conduct discontinuously, which inevitably worsens the power quality of the load voltage. When the circulating current designed under the large inductive load is applied to different load types, it is possible that the amplitude of the circulating current is greater than half of the instantaneous load current.

To set the 12-pulse rectifier with AIPR as an example, this paper analyzes the effect of circulating current on the input line current under different load types, and proposes some specific methods about how to ensure the power quality of ac and dc mains.

Manuscript received September 3, 2014; revised November 20, 2014; accepted December 24, 2014. Date of publication January 13, 2015; date of current version August 21, 2015. Recommended for publication by Associate Editor J. Biela. This work was supported in part by the National Natural Foundation of China under Grant 51107019 and 51307034, by the National Natural Foundation of Shan Dong province under Grant ZR2013EEQ002, by the Fundamental Research Funds for the Central Universities under Grant HIT.NSRIF.2013127 and HIT.NSRIF2015118.

The authors are with the Electrical Engineering and Automation, Harbin Institute of Technology, Harbin, Heilongjiang 150001, China (e-mail: mfg0327@sina.com; yangv@hit.edu.cn; zhuyihhaohao@163.com; hualeier111@126.com; syyang@hit.edu.cn).

Color versions of one or more of the figures in this paper are available online at http://ieeexplore.ieee.org.

Digital Object Identifier 10.1109/TPEL.2015.2391272

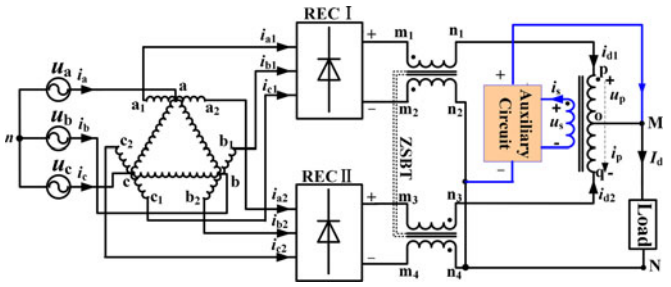

Fig. 1. Twelve-pulse rectifier with active interphase reactor.

Especially, for the *RL*-type load, we propose a new amplitude of circulating current to avoid discontinuous conduction of the bridge rectifiers; and for the *RLC*-type load, we design a *LC* filter to ensure the power quality of ac and dc mains. Because the essence of the MPRs using active reduction method is the same, the analysis of load adaptability in this paper is suitable to other MPRs.

II. Analysis of Load Adaptability

A. Principle of Active Harmonic Reduction in MPR

The 12-pulse rectifier with AIPR is illustrated in Fig. 1. In Fig. 1, a delta-connected autotransformer is used to produce two groups of three-phase voltages with 30° phase-shift angle to feed the two diode rectifiers. A zero sequence blocking transformer (ZSBT) exhibits high impedance to zero-sequence currents and can ensure the independent operation of the two rectifiers. The kVA ratings of the autotransformer and ZSBT are about 25% and 7.6% of load power, respectively [11].

Compared with the interphase reactor, the AIPR has an additional secondary winding connected in series with an auxiliary circuit. By controlling the input current of the auxiliary circuit, the output currents of two bridge rectifiers are modified actively, and the input line current of MPR is shaped further as sine wave [8], [9], [11], [14].

Fig. 2 illustrates the relation among the input and output currents of diode bridge rectifiers, the input and output voltages of diode bridge rectifiers, the input line current of 12-pulse rectifier, the load voltage and the circulating current $i_{\rm p}$ under large inductive load. Under large inductive load, the THD of input line current is about 1%.

From Fig. 2, load voltage $u_{\rm d}$ is calculated as

$$u_{\rm d} = U_{\rm d}\left(1 - \sum_{n=1}^{\infty} \frac{2}{144n^2 - 1}\cos n\pi \cos 12n\omega t\right) \tag{1}$$

where $U_{\rm d}$ is load average voltage.

From Fig. 2, the circulating current $i_{\rm p}$ meets

$$i_{\rm p} = I_{\rm d}\sum_{n=1}^{\infty} \frac{4}{n^2\pi^2}\sin\frac{3n\pi}{2}\sin 6n\omega t \tag{2}$$

where $I_{\rm d}$ is load average current, and it meets

$$I_{\rm d} = \frac{U_{\rm d}}{R}. \tag{3}$$

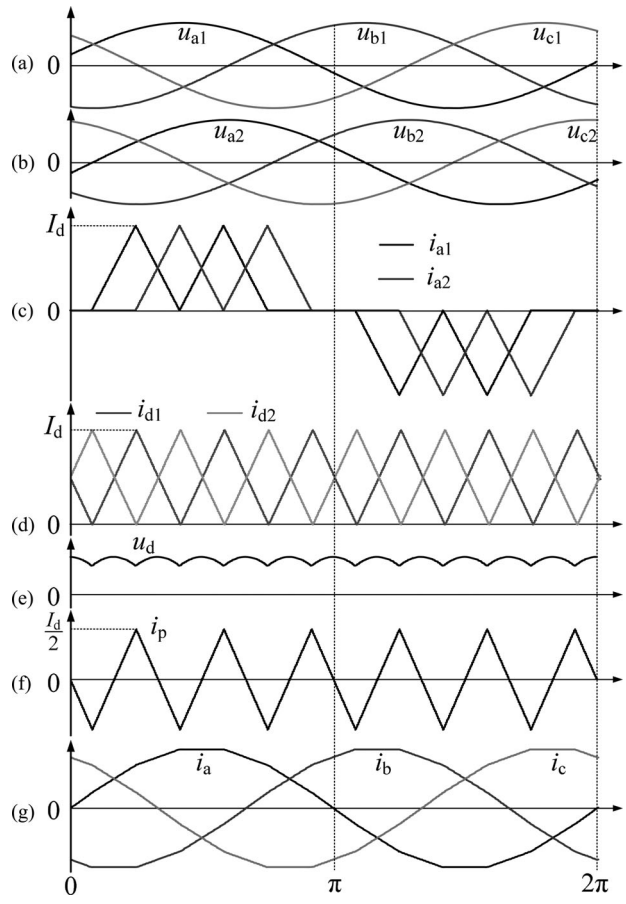

Fig. 2. (a) Input voltages of diode bridge rectifier I. (b) Input voltages of diode bridge rectifier II. (c) Input currents of the two diode bridge rectifiers. (d) Output currents of the two diode bridge rectifiers. (e) Load voltage. (f) Circulating current. (g) Input line current.

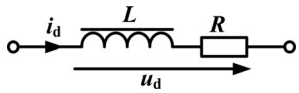

Fig. 3. Equivalent circuit of *RL*-type load.

B. RL-Type Load

The load can be equivalent to an inductor connected in series with a resistor in induction heating system [15]. Fig. 3 illustrates the equivalent circuit. Because the inductance is finite, the load current ripple cannot be filtered completely.

Load current is determined by load voltage and load type. From expression (1) and Fig. 3, load current is calculated as

$$\begin{cases} i_{\rm d} = I_{\rm d}\left[1 - \sum\limits_{n=1}^{\infty} \dfrac{2\cos(n\pi)\cos(12n\omega t - \varphi)}{(144n^2-1)\sqrt{1+(12n\omega L/R)^2}}\right] \\ \varphi = \arctan(12n\omega L/R). \end{cases} \tag{4}$$

From Fig. 1, output currents of the two bridge rectifiers can be expressed as

$$\begin{cases} i_{\rm d1} = 0.5i_{\rm d} + i_{\rm p} \\ i_{\rm d2} = 0.5i_{\rm d} - i_{\rm p}. \end{cases} \tag{5}$$

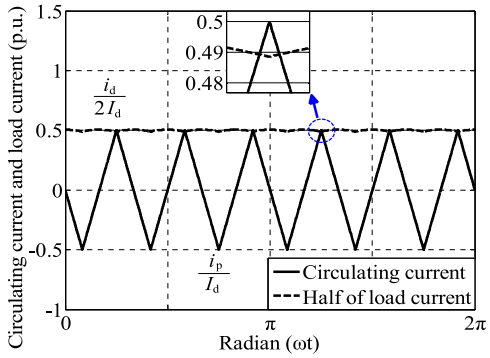

Fig. 4. Circulating current and half of load current under *RL*-type load when the ratio of ωL to R is zero.

Substituting expressions (2) and (4) into (5), the currents $i_{\mathrm{d}1}$ and $i_{\mathrm{d}2}$ are calculated as equation (6) as shown at the bottom of the page

From expressions (4) and (6), the currents i_{d}, $i_{\mathrm{d}1}$, and $i_{\mathrm{d}2}$ are determined by the ratio of ωL to R. In application, load smoothing inductance is restricted. Therefore, the load current contains ripples inevitably, and has a minimum in one cycle which is less than the circulating current designed under large inductive load. When the circulating current designed under large inductive load is used, from (5), the output currents of the two bridge rectifiers are less than zero theoretically; and in practical operation, the bridge rectifiers conduct discontinuously, and the output current of the bridge rectifiers are zero, which affects the power quality of load voltage even though the discontinuous conduction duration is very short. Therefore, the circulating current designed under large inductive load is not suitable to the *RL-type* load.

When the ratio of ωL to R is zero, the ripple of load current is maximal, and the minimum of the load current is less than that of the load current when the ratio of ωL to R is not equal to zero. Fig. 4 illustrates the circulating current and half of load current when the ratio is zero. It is observed that the circulating current near the wave crest is greater than half of load current, as shown in magnified region of Fig. 4. When the ratio of ωL to R is zero, the load is resistive, which is a special case of *RL*-type load and is the best case to show that the circulating current designed under large inductive load is not suitable.

Controlling the amplitude of the circulating current to be less than or equal to the minimum of half of load current may ensure that the bridge rectifiers operate under continuous or critical continuous condition. When $\boldsymbol{L} = 0$, the ripple of load current is maximal, and load current has a minimum i_{dmin}. If the amplitude of the design circulating current is controlled to be equal to the half of i_{dmin}, output currents of the two bridge rectifiers can be ensured to be continuous when L varies from zero to infinite.

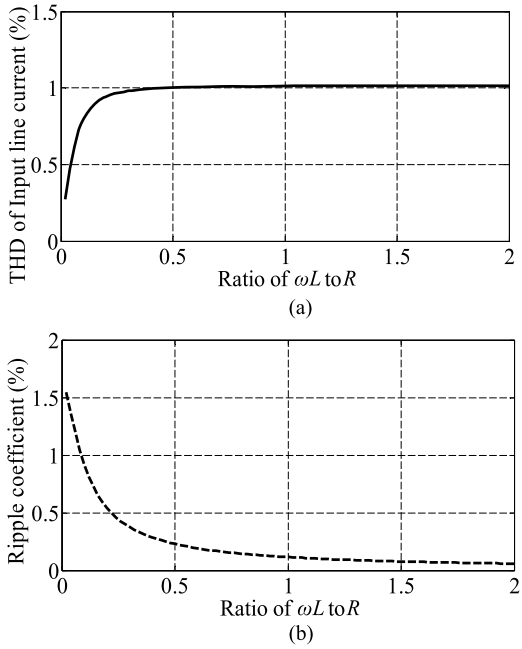

Fig. 5. (a) Relation between the THD of input line current and the ratio of ωL to R under *RL*-type load. (b) The relation between the ripple coefficient and the ratio of ωL to R under *RL*-type load.

When $\boldsymbol{L} = 0$, load current is

$$i_{\mathrm{d}} = I_{\mathrm{d}} \left[1 - \sum_{n=1}^{\infty} \frac{2\cos(n\pi)\cos(12n\omega t)}{(144n^2 - 1)} \right]. \tag{7}$$

The minimum of the load current is calculated as

$$i_{\mathrm{dmin}} = 0.977 I_{\mathrm{d}}. \tag{8}$$

Hence, the amplitude i_{pm} of the circulating current should meet

$$i_{\mathrm{pm}} = 0.5 \times 0.977 I_{\mathrm{dav}} = 0.489 I_{\mathrm{dav}}. \tag{9}$$

The required circulating current may be expressed as

$$i_{\mathrm{px}} = 0.977 I_{\mathrm{d}} \sum_{n=1}^{\infty} \frac{4}{n^2\pi^2} \sin\frac{3n\pi}{2} \sin 6n\omega t. \tag{10}$$

When the circulating current meets expression (10), the bridge rectifiers operate under continuous condition for *RL*-type load.

The ripple coefficient of load current can be defined by

$$k_{\mathrm{d}} = \frac{i_{\mathrm{d\,max}} - i_{\mathrm{d\,min}}}{2I_{\mathrm{d}}} \tag{11}$$

where i_{dmax} is the maximum of load current.

$$\begin{cases} i_{\mathrm{d}1} = \dfrac{I_{\mathrm{d}}}{2} \left[1 + \displaystyle\sum_{n=1}^{\infty} \frac{8}{n^2\pi^2} \sin\frac{3n\pi}{2} \sin 6n\omega t - \sum_{n=1}^{\infty} \frac{2\cos(n\pi)\cos(12n\omega t - \varphi)}{(144n^2 - 1)\sqrt{1 + (12n\omega L/R)^2}} \right] \\ i_{\mathrm{d}2} = \dfrac{I_{\mathrm{d}}}{2} \left[1 - \displaystyle\sum_{n=1}^{\infty} \frac{8}{n^2\pi^2} \sin\frac{3n\pi}{2} \sin 6n\omega t - \sum_{n=1}^{\infty} \frac{2\cos(n\pi)\cos(12n\omega t - \varphi)}{(144n^2 - 1)\sqrt{1 + (12n\omega L/R)^2}} \right] \end{cases} \tag{6}$$

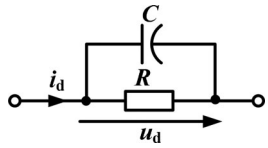

Fig. 6. Equivalent circuit of *RC*-type load.

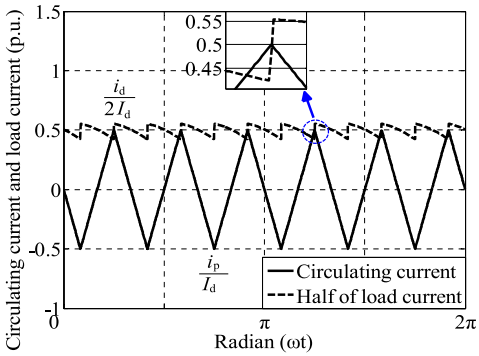

Fig. 7. Circulating current and half of load current when $\omega RC = 0.1$.

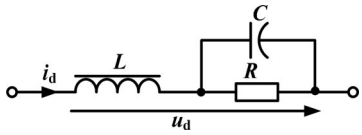

Fig. 8. Equivalent circuit of *RLC*-type load.

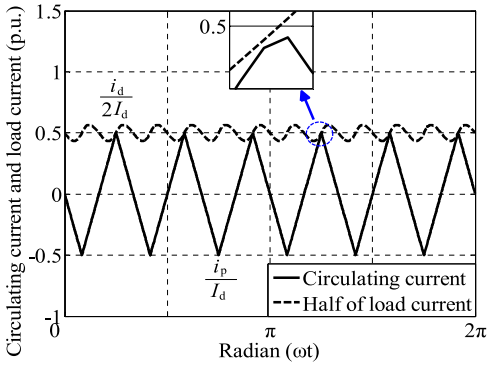

Fig. 9. Circulating current and half of load current for *RLC*-type load when ωRC is 6, and the ratio of ωL to R is 0.01.

Fig. 5 illustrates the effect of load parameter (ratio of ωL to R) on THD of input line current, and ripple coefficient of load current.

From Fig. 5, the ripple coefficient decreases as the ratio of ωL *to* R increases. Conversely, THD of input line current increases as the ratio increases. When ratio is equal to zero, the ripple coefficient is maximum, and the THD is minimum. When the ratio reaches a certain value, THD is stable around 1, and ripple coefficient is about 0.06%.

Therefore, reducing slightly the amplitude of the circulating current not only can ensure the normal operation of bridge rectifiers, but also can ensure harmonic reduction ability of the 12-pulse rectifier with AIPR under *RL*-type load.

C. RC-Type Load

When a large capacitor is connected in parallel with load, the load can be equivalent as *RC*-type, as shown in Fig. 6.

For *RC*-type load, load current is calculated as equation (12) as shown at the bottom of the page

Fig. 7 illustrates the circulating current and half of load current when the circulating current meets expression (2) and ωRC is equal to 0.1. It is observed that discontinuous operation time interval of bridge rectifier is longer than that of the resistive load. With the increase of capacitance, the ripple amplitude of half of load current also increases resulting in the increase of discontinuous conduction time. Although reducing the amplitude of the circulating current can ensure the continuous conduction of bridge rectifiers, considerably decreasing the amplitude may depress harmonic reduction ability. Therefore, the circulating current designed under large inductive load is not suitable for the *RC*-type load.

D. RLC-Type Load

Due to the leakage inductance of magnetic devices, such as autotransformer and AIPR, there is no *RC*-type load in practical application. Most of load can be equivalent to be the *RLC*-type load, as shown in Fig. 8. For example, when load is a high-power dc–dc converter, or a dc–ac converter, a *LC* filter is connected to the output side of MPR at the front of converter. If the converter is connected in parallel with capacitor directly, the leakage inductance of magnetic devices can be viewed as the load inductance L. Therefore, the equivalent circuit shown in Fig. 8 is commonly used in application, and can be viewed as a resistance connected with a *LC* filter.

$$\begin{cases} i_{\mathrm{d}} = I_{\mathrm{d}}[1 - \sum\limits_{n=1}^{\infty} \dfrac{2\sqrt{1+(12n\omega RC)^2}}{144n^2-1}\cos(n\pi)\cos(12n\omega t - \varphi)] \\ \varphi = -\arctan(12n\omega RC). \end{cases} \tag{12}$$

$$\begin{cases} i_{\mathrm{d}} = I_{\mathrm{d}}\left[1 - \sum\limits_{n=1}^{\infty} \dfrac{2\cos(n\pi)\cos(12n\omega t - \varphi)\sqrt{1+(12n\omega RC)^2}}{(144n^2-1)\sqrt{[(1-(12n\omega)^2 LC)]^2 + (12n\omega L/R)^2}}\right] \\ \varphi = \arctan\left[\dfrac{12n\omega L/R}{1-(12n\omega)^2 LC}\right] - \arctan(12n\omega RC) \end{cases} \tag{13}$$

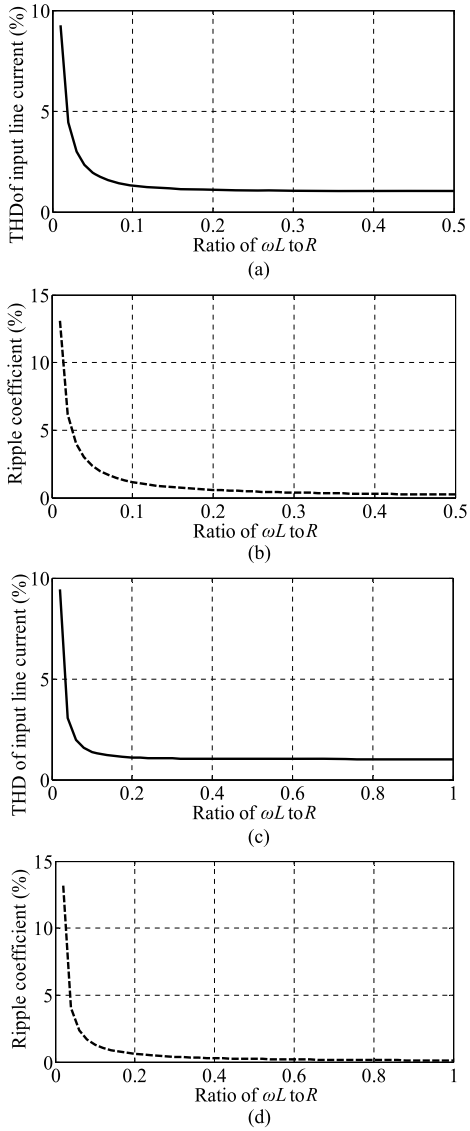

Fig. 10. THD and ripple coefficient for *RLC*-type load under different ratios of ωL to R. (a) THD of input line current when $\omega RC = 6$. (b) Ripple coefficient of load current when $\omega RC = 6$. (c) THD of input line current when $\omega RC = 0.6$. (d) Ripple coefficient of load current when $\omega RC = 0.6$.

When load voltage meets expression (1) for the *RLC*-type load, load current is calculated as equation (13) as shown at the bottom of the previous page

From expression (13), load current ripple is correlative with the load parameter ωRC and the ratio of ωL to R. Fig. 9 illustrates the circulating current and half of load current when ωRC is equal to 6, and the ratio of ωL to R is 0.01. In Fig. 9, owing to the phase-shift effect of *LC* filter on load current ripple, the wave crest of circulating current and half of load current do not intersect. Therefore, if the circulating current is controlled to meet expression (2), the bridge rectifiers can operate under continuous condition.

Fig. 10 illustrates the THD of input line current and ripple coefficient of load current under different ratios of to ωL to R. When the ratio is less, load current ripple is more resulting in more harmonic of input line current. With the increase of the ratio, ripple coefficient of load current decreases, and the THD also decreases rapidly. When the ratio reaches a certain

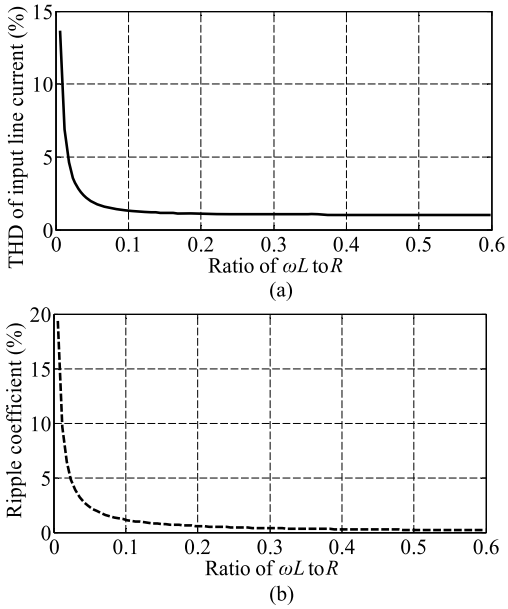

Fig. 11. (a) Relation between the THD of input line current and the ratio of ωL to R under *RLC*-type load. (b) The relation between the ripple coefficient and the ratio of ωL to R under *RLC*-type load.

interval, the ripple coefficient keeps on decreasing, but the THD maintains about 1%.

Fig. 10 indicates that the *LC* filter affects the THD and ripple coefficient. Although a large inductance L filter may increase the cost and size, resulting in less harmonics of input line current and load current ripple. In addition, from Fig. 2, the circulating current produced by the auxiliary circuit only affects the input line current of MPR, but does not affects the load voltage. Therefore, in order to ensure the power quality of load side, it is also necessary to install a *LC* filter.

From Fig. 2, load voltage is dc voltage with 12 pulses. Therefore, *LC* filter is required to ensure that the voltage across capacitor does not contain 12 times low-frequency ripple. The *LC* filter should meet

$$\frac{1}{2\pi\sqrt{LC}} \ll 600 \text{ Hz}. \tag{14}$$

Generally, output side of *LC* filter is connected with a high-power high-frequency dc–dc converter or a dc–ac converter. Therefore, the capacitance $\boldsymbol{C}$ should be large enough to eliminate the high-frequency voltage ripple.

Assume that the low-frequency voltage ripple across the capacitor is zero, twelve times ac component of load voltage will be across the inductor L. The voltage across the inductor L meets

$$u_{\mathrm{L}} = L\frac{\mathrm{d}i_{\mathrm{d}}}{\mathrm{d}t} = -U_{\mathrm{d}}\sum_{n=1}^{\infty}\frac{2}{144n^2-1}\cos n\pi\cos 12n\omega t. \tag{15}$$

Load current is calculated as

$$\begin{aligned} i_{\mathrm{d}} &= \frac{U_{\mathrm{d}}}{R} - \frac{U_{\mathrm{d}}}{\omega L}\sum_{n=1}^{\infty}\frac{1}{6n(144n^2-1)}\cos n\pi\sin 12n\omega t \\ &= I_{\mathrm{d}}\left[1 - \frac{R}{\omega L}\sum_{n=1}^{\infty}\frac{1}{6n(144n^2-1)}\cos n\pi\sin 12n\omega t\right]. \end{aligned} \tag{16}$$

From expression (16), load current i_{d} is only related to load resistance R and load inductance L. According to expressions

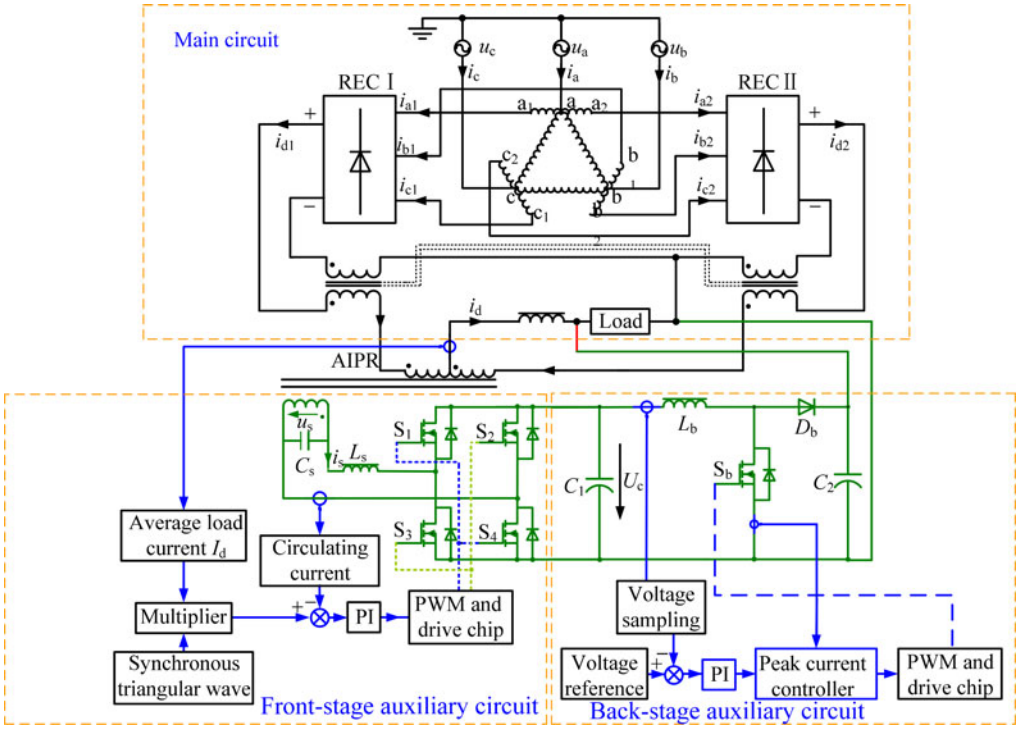

Fig. 12. Control block diagram of the proposed MPR with two-stage auxiliary circuit.

(2), (5), and (16), Fig. 11 illustrates the THD of input line current and ripple coefficient of load current under different ratios of ωL *to* R.

From Fig. 11, when the ratio is less than 0.1, both the THD and ripple coefficient are large. When the ratio is greater than 0.2, the THD is reduced to about 1%. Although continually increasing the ratio can decrease the ripple coefficient, it has little effect on the THD.

The inductance L is determined by the kVA rating of MPR. For the load with a fixed power, the inductance L can be chosen conveniently according to the requirement of THD and ripple coefficient. When resistance R increases, the ratio of ωL to R decreases correspondingly, which causes the increase of the THD and ripple coefficient inevitably. Although the reasonable inductance L can ensure the less THD value for *RLC*-type load under related output power, variation of output power may cause negative effect on input line current and load current. Therefore, in order to ensure the harmonic reduction ability when the output power varies in a large range, it is necessary to choose a large inductance L.

Summarily, the *LC* filter can be designed as follows. First, choose the capacitance C large enough to delete the high-frequency voltage ripple. Afterward, ascertain the range of inductance L according to expression (14), and then choose an appropriate inductance L according to the requirement of THD when output power varies.

III. Simulation and Experimental Validation of Load Adaptability

In order to validate the aforementioned theoretical analysis, some simulation and experimental results are presented in this

TABLE I
Parameters of the MPR and Auxiliary Circuit

Parameter	Value
Load voltage U_d	400 V
Load current I_d	16 A
Input line voltage U	280 V
Line frequency	50 Hz
Output power P_o	6.4 kW
Turn ratio of AIPR	1:1
The front stage inductor L_s	1 mH
The front stage switching frequency	50 kHz
The back stage inductor L_b	350 μH
The back stage switching frequency	50 kHz

A. Auxiliary Circuit

There are several topologies which are able to realize the function of auxiliary circuit. For example, in [8], Choi *et al.* proposed an auxiliary circuit with a single-phase half bridge PWM rectifier. The single-phase half bridge PWM rectifier can be considered as a single-stage auxiliary circuit, and it has simple control circuit, fast dynamic response, good stability. However, some shortcomings of the single-stage auxiliary circuit were observed in application. In the single-stage auxiliary circuit, the input current of the PWM rectifier is proportional to load current, and its output voltage is passively equal to the load voltage. Therefore, input current of the rectifier and its output voltage interact with each other, and it is difficult to obtain the required circulating current when the input voltage of MPR, or load current varies. In [11], Lee *et al.* proposed a two-stage auxiliary circuit with a diode bridge rectifier and a single-phase boost PFC to control the amplitude and phase of circulating current, respectively. However, because the diode bridge rectifier is

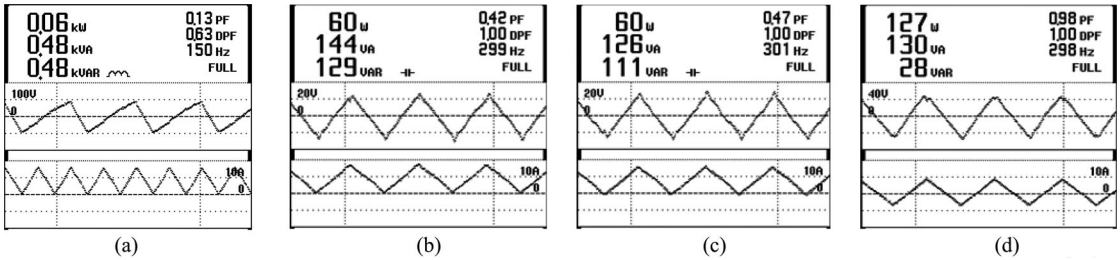

Fig. 13. kVA rating of the magnetic devices. (a) kVA rating of ZSBT. (b) Winding op of the primary winding. (c) Winding oq of primary winding. (d) The secondary winding.

uncontrolled, the input current of the auxiliary circuit cannot be controlled precisely. Therefore, when the input voltage of MPR, or load current varies, it is also difficult to precisely obtain the required circulating current. In order to avoid the aforementioned shortcomings, in this paper, we propose a two-stage auxiliary circuit which is the combination of PWM converter and boost converter, as shown in Fig. 12. In Fig. 12, the front stage of the auxiliary circuit is a PWM rectifier, and the back stage is a Boost converter. The front stage contains a current control loop, which is only used to obtain the required circulating current precisely. When load current or input voltages changes suddenly, the current transformer detects the change, and sends the new current signal into multiplier (AD532) to produce the corresponding synchronous reference triangular wave signal accordingly. The error between the detected circulating current and the reference signal is sent into the PI controller, and the output signal of PI controller is sent into PWM chip (UC3637) and drive chip (IR2110) to produce the drive signal to drive the PWM rectifier. The PWM rectifier regulates the amplitude of circulating current to ensure the harmonic content in a low level.

The back stage contains a voltage control loop, which is used to control the output voltage of the front stage to be equal to the load voltage. The voltage reference signal of the back stage is calculated according to the input voltage and input current of MPR, and voltage across the secondary winding of active IPR. The peak current controller (UC3846) adjusts the output signal of the PI regulator and current sample signal of MOSFET $S_{\rm b}$ to produce the PWM signal. The PWM signal is send to drive chip TLP250 to drive the MOSFET.

Although the energy conversion efficiency of the two-stage auxiliary circuit may be reduced due to the application of the two stages circuit, effect of power losses resulting from the two-stage auxiliary circuit on energy conversion coefficient of MPR is minor because the kVA rating of the two-stage auxiliary circuit is only 3% of output power of MPR.

An experimental setup is built to verify the theoretical analysis and function of the proposed two-stage auxiliary circuit. Table I shows the parameters of the MPR and auxiliary circuit for experiment.

B. KVA Rating of the ZSBT, IPR, and the Delta-Connected Autotransformer

The autotransformer, active IPR, and ZSBT are the main magnetic decvices of MPR. When the auxiliary circuit is applied, the circulating current may affects the kVA rating of the magnetic device. Fig. 13(a) shows the voltage across and current through the ZSBT. The kVA rating of ZSBT is about 480 VA accounting for 7.5% of output power.

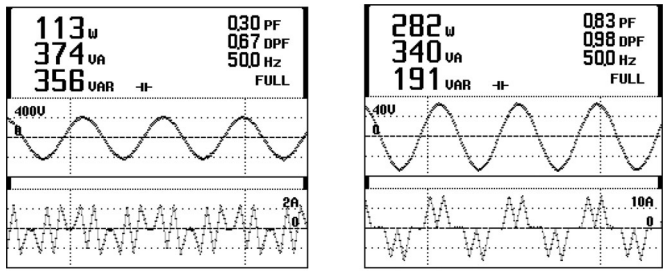

Fig. 14. KVA rating of the autotransformer. (a) TWinding ab. (b) Winding aa1.

Fig. 13(b)–(d) shows the voltage across and current through the windings of active IPR. From Fig. 13(b)–(d), the kVA rating of AIPR is calculated as

$$\begin{aligned} S_{\rm AIPR} &= 0.5 \times (144 + 126 + 130) \\ &= 200 \text{ VA} \approx 3.1\% P_{\rm o}. \end{aligned} \tag{17}$$

In Fig. 13(d), the amplitudes of the voltage and current are about 49 V and 8 A, respectively. The current and voltage are symmetrical triangular wave with frequency 300 Hz, and are in phase. The kVA rating of the secondary winding is 130 VA accounting for only about 2% of output power, which indicates about 130 VA harmonic power is absorbed by the auxiliary circuit through the secondary winding.

Fig. 14 illustrates the voltage across and current through the winding of autotransformer. Assume that the autotransformer is symmetrical, the kVA rating of the autotransformer is calculated as

$$\begin{aligned} S_{\rm tran} &= 0.5 \times (3 \times 374 + 6 \times 340) \\ &= 1581 \text{ VA} \approx 24.7\% P_{\rm o}. \end{aligned} \tag{18}$$

From (18), the kVA rating of the autotransformer is about 24.7% of output power. Therefore, the total kVA of the three devices is 35.3% of output power. Table II shows the comparison of the kVA ratings of the three magnetic devices in the 12-pulse rectifier and 12-pulse rectifier using AIPR.

From Table II, after using the auxiliary circuit, the kVA ratings of the all three magnetic devices increases. Because the auxiliary circuit only modulates the current, but not affects the voltage, the increase of kVA rating is due to the increase of current through the windings.

TABLE II
COMPARISON OF KVA RATING OF THE MAGNETIC DEVICE IN THE 12-PULSE RECTIFIER AND 12-PULSE RECTIFIER USING AIPR (EXPERIMENTAL RESULTS)

System	Transfomer	ZSBT	AIPR
Using AIPR	24.7%P_o	7.5% P_o	3.1% P_o
Not using AIPR	18.4%P_o	6.61% P_o	2.04% P_o

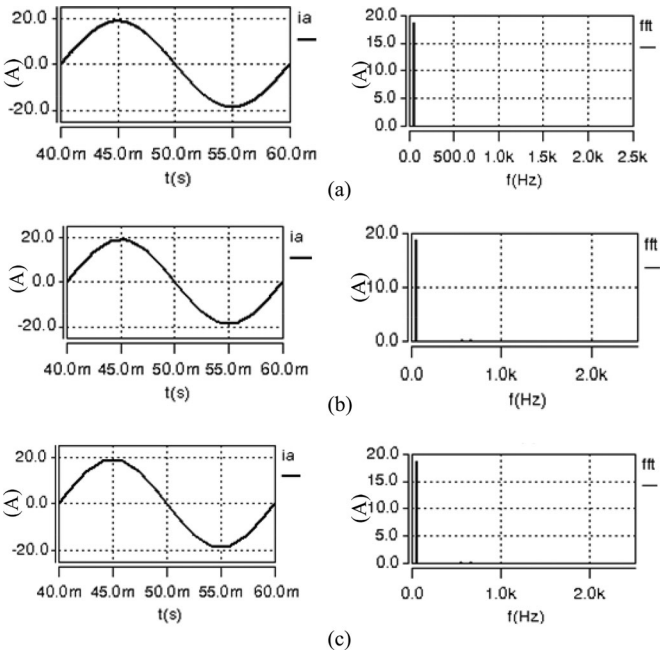

Fig. 15 Input line current and its spectrum. (a) Ratio of ωL to R is zero, THD = 0.2%. (b) Ratio of ωL to R is 0.1, THD = 0.8%. (c) Ratio of ωL to R is 1, THD = 1.1%. (Simulation results).

TABLE III
HARMONICS COMPARISON OF THE 12-PULSE RECTIFIER USING THE PROPOSED AUXILIARY CIRCUIT UNDER DIFFERENT RATIOS OF ωL TO R (SIMULATION RESULTS)

Ratio of ωL to R	11th	13th	23rd	25th	THD
0	0.0020	0.0015	0.0006	0.0005	0.2%
0.1	0.0042	0.0066	0.0006	0.0026	0.8%
1	0.0045	0.0086	0.0002	0.0030	1.1%

C. Simulation and Experimental Results for RL-Type Load

Fig. 15 illustrates the input line current and their spectrums for *RL*-type load under different ratios of ωL to R, and Table III shows the harmonics normalized by the fundamental components. When simulating, the amplitude of circulating current is controlled to meet expression (10). Fig. 15 indicates that THD of input line current increases as the inductance L, but the THD is small always. The results also indicate indirectly that load current ripple has positive effect on harmonic reduction of input line current for *RL*-type load. The consistence of simulation result and theoretical analysis shows the 12-pulse rectifier with AIPR is suitable for *RL*-type load.

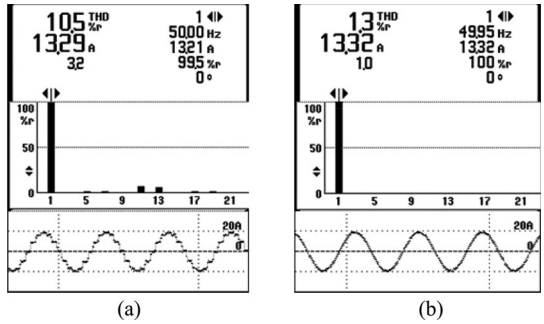

Fig. 16. Input line current and its spectrum under *RL*-type load. (a) 12-pulse rectifier. (b) 12-pulse rectifier with the proposed auxiliary circuit. (Experimental results).

TABLE IV
HARMONICS COMPARISON OF THE 12-PULSE RECTIFIER AND THE 12-PULSE RECTIFIER USING THE PROPOSED AUXILIARY CIRCUIT UNDER *RL*-TYPE LOAD (EXPERIMENTAL RESULTS)

	5th	7th	11th	13th	23rd	25th	THD
AIPR	0	0	0.002	0.011	0.001	0.004	1.3%
12-pulse	0.020	0.018	0.084	0.068	0.030	0.016	10.5%

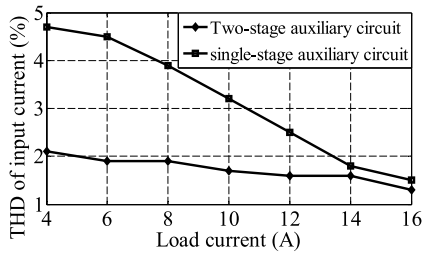

Fig. 17. THD comparison of the 12-pulse rectifier with two-stage and single-stage auxiliary circuit.

When load inductance L is equal to 12 mH, Fig. 16(a) and (b) shows the input line current and its spectrum of the 12-pulse rectifier without and with the auxiliary circuit, respectively; and Table IV shows their comparison of harmonic content normalized by fundamental component. When the proposed auxiliary circuit is used, the harmonics in input line current is eliminated effectively.

Fig. 17 illustrates THD comparison of the 12-pulse rectifier using two-stage and single-stage auxiliary circuit when load current changes from 4 to 16 A. The experimental results indicate the proposed MPR has good load adaptability to variation of output power.

When the load rsistance is changed from 80 to 40 Ω, Fig. 18 illustrates the system dynamic response when load current changes suddenly from 5 to 10 A. In Fig. 18, the lines from top to bottom are average load current, input line current, and input current of the auxiliary circuit, respectively. From Fig. 18, the time response is about 30 ms.

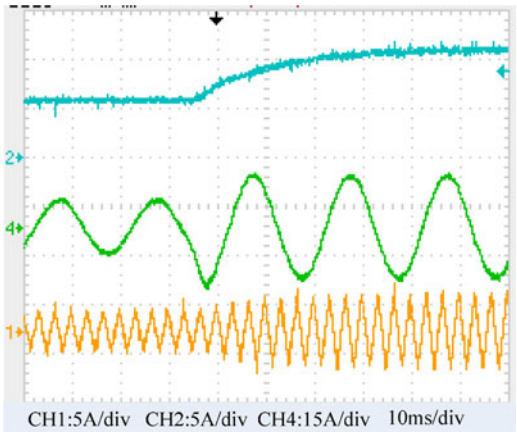

Fig. 18. System dynamic response when load current changes suddenly.

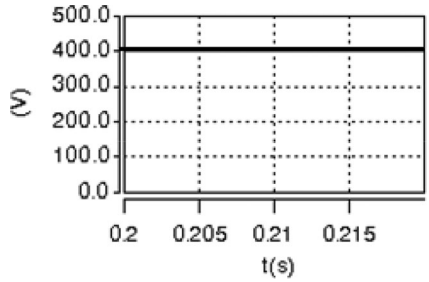

Fig. 19. Voltage across the capacitance C.

D. Simulation and Experimental Results for RLC-Type Load

Under the same load average voltage and load resistance, the simulation for *RLC*-type load is carried out. When simulating, load resistance R is 25 Ω, inductance L is 12 mH, and capacitance $\boldsymbol{C}$ is 1125 μF. It is calculated that the ratio of ωL to R is 0.15, and $1/2\pi\sqrt{LC} \approx 43\,\text{Hz} \ll 600\,\text{Hz}$. Fig. 19 shows the voltage across the capacitance $\boldsymbol{C}$. It is observed from Fig. 19 that the twelve times voltage ripple is filtered completely.

Whenthe load resistance changes, Fig. 20 illustrates the input line current and its spectrum under the same *LC* filter, and Table V shows their comparison of harmonic content normalized by fundamental component.

Fig. 20(a) indicates that the *LC* filter can ensure the harmonic reduction ability under the related output power. Fig. 20(b) and (c) illustrates the input line currents and spectrums under half load and quarter load, respectively, which indicate both the THD and ripple coefficient increase as the output power decreases. Although a larger inductance L means better load adaptability to variation of ouput power, the least inductance L should be designed in application according to the requirement of THD. Therefore, appropriate *LC* filter can ensure the proposed MPR has good performance.

Fig. 21 illustrates THD comparison of the 12-pulse rectifier using the two-stage and single-stage auxiliary circuit when load current changes from 4 to 16 A. When the resistance is 25 Ω (the related output power), the THD is about 1.3%. However, load current ripple increases as load resistance increases, which may depress the harmonic reduction ability of the proposed MPR.

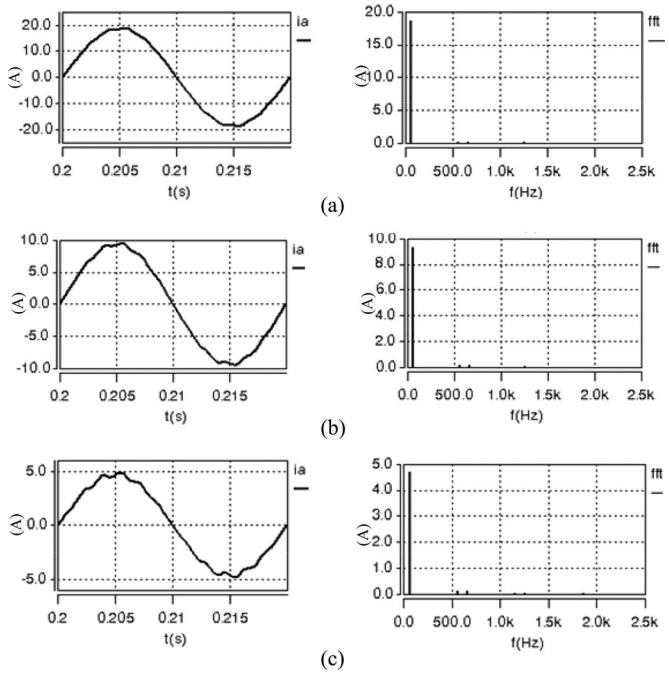

Fig. 20. Input line current and its spectrum. (a) Ratio of ωL to R is 0.1, THD = 1.3%. (b) Ratio of ωL to R is 0.05, THD = 2.0%. (c) Ratio of ωL to R is 0.025, THD = 3.5%.

TABLE V
HARMONICS COMPARISON OF THE 12-PULSE RECTIFIER USING THE PROPOSED AUXILIARY CIRCUIT UNDER DIFFERENT RATIOS OF ωL TO R FOR *RLC*-TYPE LOAD (SIMULATION RESULTS)

Ratio of ωL to R	11th	13th	23rd	25th	THD
0.1	0.0067	0.0118	0.0012	0.0041	1.3%
0.05	0.0128	0.0149	0.0017	0.0043	2.0%
0.025	0.0251	0.0235	0.0028	0.0050	1.1%

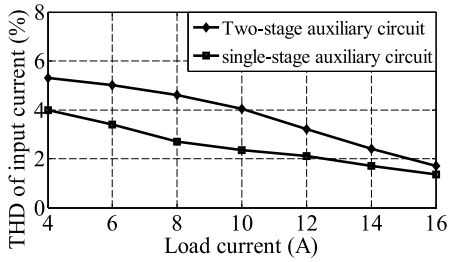

Fig. 21. THD of input line current under different load currents for *RLC*-type load.

Therefore, compared with the *RL*-type load, the proposed MPR cannot maintain the THD in a low level for *RLC*-type load when load resistance varies. In order to keep the THD when load resistance varies in a large range, it is necessary to design a large inductance according to Fig. 11.

From Fig. 21, the experimental results indicate the proposed MPR has good load adaptability to variation of output power under the *RLC*-type load.

IV. Conclusion

This paper analyzes the load adaptability of 12-pulse rectifier with AIPR. Some conclusions are obtained as follows:

1) Under *RL*-type load, if the circulaitng current designed under large inductive load is applied, the two diode bridge rectifiers conduct discontinuously, which depresss the power quality of load voltage. To ensure the continuous conduction of the two diode bridge rectifiers, the amplitude of the circulating current should be equal to half of minimum of load current when the load is purely resistive.
2) The active harmonic reduction of MPR is not suitable to *RC*-type load.
3) For *RLC*-type load, the load inductance L and load capacitance C are considerd as a *LC* filter. In order to obtain the required system performance, the load inductance L should be determined by the ratio of ωL to load resistance under slight load.
4) A 12-pulse rectifier using two-stage auxiliary circuit is proposed. Compared with the 12-pulse rectifier using single-stage auxiliary circuit, the proposed rectifier has better load adaptability and harmonic elimination ability. Some simulation and experiment are carried out to verify the correctness of theoretical analysis under *RL*-type load and *RLC*-type load.

References

[1] J. Sun, Z. Bing, and K. J. Karimi, "Input impedance modeling of multipulse rectifiers by harmonic linearization," *IEEE Trans. Power Electron.*, vol. 24, no. 12, pp. 2812–2820, Dec. 2009.

[2] B. Singh, S. Gairola, B. N. Singh, A. Chandra, and K. Al-Haddad, "Multipulse AC-DC converters for improving power quality: a review," *IEEE Trans. Power Electron.*, vol. 23, no. 1, pp. 260–281, Jan. 2008.

[3] Y. Shiyan, M. Fangang, and Y. Wei, "Optimum design of inter-phase reactor with double-tap-changer applied to multi-pulse diode rectifier," *IEEE Trans. Ind. Electron.*, vol. 57, no. 9, pp. 3022–3029, Sep. 2010.

[4] M. S. Hamad, M. I. MAsoud, and B. W. Williams, "Medium-voltage 12-pulse converter: Output voltage harmonic compensation using a series APF," *IEEE Trans. Ind. Electron.*, vol. 61, no. 1, pp. 43–52, Jan. 2014.

[5] R. Kalpana, G. Bhuvaneswari, and B. Singh, "Autoconnected-transformer-based 20-pulse AC-DC converter for telecommunication power supply," *IEEE Trans. Ind. Electron.*, vol. 60, no. 10, pp. 4178–4190, Oct. 2013.

[6] B. Singh, V. Garg, and G. Bhuvaneswari, "A novel T-connected autotransformer-based 18-pulse AC–DC converter for harmonic mitigation in adjustable-speed induction-motor drives," *IEEE Trans. Ind. Electron.*, vol. 54, no. 5, pp. 2500–2511, Oct. 2007.

[7] I. Araujo-Vargas, A. J. Forsyth, and F. J. Chivite-Zabalza, "Capacitor voltage-balancing techniques for a multipulse rectifier with active injection," *IEEE Trans. Ind., Appl.*, vol. 47, no. 1, pp. 185–198, Jan./Feb. 2011.

[8] S. Choi, P. N. Enjeti, H. H. Lee, and I. J. Pitel, "A new active interphase reactor for 12-pulse rectifiers provides clean power utility interface," *IEEE Trans. Ind. Appl.*, vol. 32, no. 6, pp. 1304–1311, Nov./Dec. 1996.

[9] F. Meng, W. Yang, and S. Yang, "Active harmonic suppression of paralleled 12-pulse rectifier at DC side," *Sci. China: Technological Sci.*, vol. 54, no. 12, pp. 3320–3331, Dec. 2011.

[10] M. E. Villablanca, J. I. Nadal, and M. A. Bravo, "A 12-pulse AC-DC rectifier with high-quality input/output waveforms," *IEEE Trans. Power Electron.*, vol. 22, no. 5, pp. 1875–1881, Sep. 2007.

[11] B. S. Lee, J. Hahn, and P. N. Enjeti, "A robust three-phase active power factor correction and harmonic reduction scheme for high power," *IEEE Trans. Ind. Electron.*, vol. 46, no. 3, pp. 483–494, Jun. 1999.

[12] F. Meng, W. Yang, and S. Yang, "Effect of voltage transformation ratio on the kilovoltampere rating of delta-connected Autotransformer for 12-pulse rectifier system," *IEEE Trans. Ind. Electron.*, vol. 60, no. 9, pp. 3579–3588, Sep. 2013.

[13] J. R. Rodriguez *et al.*, "Large current rectifiers: state of the art and future trends," *IEEE Trans. Ind. Electron.*, vol. 52, no. 3, pp. 738–746, Jun. 2005.

[14] S. Bai and S. M. Lukic, "New method to achieve AC harmonic elimination and energy storage integration for 12-pulse diode rectifiers," *IEEE Trans. Ind. Electron.*, vol. 60, no. 7, pp. 2547–2554, Jun. 2013.

[15] O. Lucía, P. Maussion, E. J. Dede, and J. M. Burdío, "Induction heating technology and its applications: past development, current technology, and future challenges," *IEEE Trans. Ind. Electron.*, vol. 61, no. 5, pp. 2509–2520, May 2014.

[16] J. Biela, D. Hassler, J. Schönberger, and J. W. Kolar, "Closed-loop sinusoidal input-current shaping of 12-pulse autotransformer rectifier unit with impressed output voltage," *IEEE Trans. Power Electron.*, vol. 26, no. 1, pp. 249–259, Jan. 2011.

[17] F. Meng, L. Gao, S. Yang, and W. Yang, "Effect of single-phasing on multipulse rectifier with active interphase reactor," *IEEE Trans. Power Electron.*, vol. 30, no. 5, pp. 2549–2555, Jan. 2015.

[18] R. Kalpana, G. Bhuvaneswari, and B. Singh, "Autoconnected-transformer -based 20-pulse AC-DC converter for telecommunication power supply," *IEEE Trans. Ind. Electron.*, vol. 60, no. 10, pp. 4178–4190, Oct. 2013.

[19] H. Akagi and K. Isozaki, "A hybrid active filter for a three-phase 12-pulse diode rectifier used as the front end of a medium-voltage motor drive," *IEEE Trans. Power Electron.*, vol. 27, no. 1, pp. 69–77, Jan. 2012.

[20] C.-M. Young, M.-H. Chen, C.-H. Lai, and D.-C. Shih, "A novel active interphase transformer scheme to achieve three-phase line current balance for 24-pulse converter," *IEEE Trans. Power Electron.*, vol. 27, no. 4, pp. 1719–1731, Apr. 2012.

[21] C.-M. Young, S.-F. Wu, W.-S. Yeh, and C.-W. Yeh, "A DC-side current injection method for improving AC line condition applied in the 18-pulse converter system," *IEEE Trans. Power Electron.*, vol. 29, no. 1, pp. 99–109, Jan. 2014.

[22] S. Singh and B. Singh, "Optimized passive filter design using modified particle swarm optimization algorithm for a 12-pulse converter-fed LCI–synchronous motor drive," *IEEE Trans. Ind., Appl.*, vol. 50, no. 4, pp. 2681–2689, Jul./Aug. 2014.

[23] A. Di Gerlando, G. M. Foglia, M. F. Iacchetti, and M. Ubaldini, "Optimized coil arrangement in wound interphase reactors for high-power rectifier systems," *IEEE Trans. Energy Convers.*, vol. 29, no. 3, pp. 652–662, Sep. 2014.

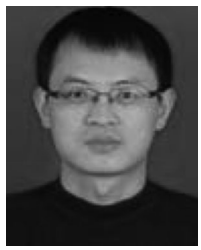

Fangang Meng was born in Shandong, China, in 1982. He received the B.S. degree in thermal energy and power engineering in 2005, and the M.S. and the Ph.D. degrees in electrical engineering from Harbin Institute of Technology, Harbin, China, in 2007 and 2011, respectively.

He is currently an Associate Professor with Harbin Institute of Technology. His research interests include harmonic detection, stability analysis of converter, high power rectification.

Wei Yang (M'09) was born in Heilongjiang, China, in 1978. He received the B.S., M.S., and Ph.D. degrees in electrical engineering from Harbin Institute of Technology, Harbin, China, in 2001, 2005, and 2010, respectively.

He is currently an Associate Professor at Harbin Institute of Technology. His current research interests include high power rectifiers.

Yi Zhu was born in Anhui, China, in 1988. He received the B.S. and M.S. degrees in electrical engineering from Harbin Institute of Technology, Harbin, China, in 2009, 2011, respectively.

He is currently an Engineer in Shanghai Research and Design Center of Carrier, Shanghai, China. His current research interests include power electronics and motor drives.

Lei Gao was born in Hebei, China, in 1982. She received the B.S., M.S., and the Ph.D. degrees in electrical engineering from Harbin Institute of Technology, Harbin, China, in 2005, 2007, and 2012, respectively.

She is currently a Lecturer at Harbin Institute of Technology. Her current research interests include power electronics and motor drives.

Shiyan Yang was born in Heilongjiang, China, in 1962. He received the B.S. and M.S. degrees in electrical engineering from the Harbin Institute of Technology, in 1984 and 1989, respectively, and the Ph.D. degree in welding engineering from the Harbin Institute of Technology, Harbin, China, in 1998.

He is currently a Professor and a Supervisor for Doctoral Candidates in Harbin Institute of Technology. He has published more than 60 papers. His research interests include high-power special type power supply and its application, energy storage system and its equilibrium, fundamental theory of finity power supply drive and key commonsense problem.